Hindawi
Geofluids
Volume 2021, Article ID 2448044, 12 pages
https://doi.org/10.1155/2021/2448044

Research Article

Experimental Study on the Characteristics of Adsorbed Gas and Gas Production in Shale Formations

Zhiming Hu,[1] Xianggang Duan,[1] Nan Shao,[1] Yingying Xu,[1,2] Jin Chang,[1] Rui Shen,[1] and Xueke Chen[1]

[1]*PetroChina Research Institute of Petroleum Exploration and Development, Langfang, Hebei 065007, China*
[2]*University of Chinese Academy of Sciences, Beijing 100049, China*

Correspondence should be addressed to Xianggang Duan; duanxg69@petrochina.com.cn
and Yingying Xu; xuyingying01@petrochina.com.cn

Received 14 May 2021; Revised 28 May 2021; Accepted 10 August 2021; Published 6 September 2021

Academic Editor: Feng Yang

Adsorbed gas and free gas both exist in shale reservoirs simultaneously due to the unique nanoscale pore structure, resulting in the complex flow mechanism of gas in the reservoir during the development process. The dynamic performance analysis of shale reservoirs has mostly been conducted by the numerical simulation and theoretical model, while the physical simulation method for relevant research is seen rarely in the literature. Thus, in this paper, an experiment system was designed to simulate the degraded development experiments of shale, coal, and tight sandstone to reveal the output law of gas in different occurrence states of shale reservoirs and clarify the pressure propagation rules of different reservoirs, and then, adsorption gas and free gas production laws were studied by theoretical models. Research indicated the following: (1) The gas occurrence state is the main factor that causes the difference of the pressure drop rate and gas production law of shale, coal, and tight sandstone. During the early stage of the development of shale gas, the free gas is mainly produced; the final contribution of free gas production can reach more than 90%. (2) The static desorption and dynamic experiments confirm that the critical desorption pressure of adsorbed gas is generally between 12 and 15 MPa. When the gas reservoir pressure is lower than the critical desorption pressure in shale and coal formation, desorption occurs. Due to the slow propagation of shale matrix pressure, desorption of adsorbed gas occurs mainly in the low-pressure region close to the fracture surface. (3) The material balance theory of closed gas reservoirs and the one-dimensional flow model of shale gas have subsequently validated the production performance law of adsorbed gas and free gas by the physical simulation. Therefore, in the practical development of shale gas reservoirs, it is recommended to shorten the matrix supply distance, reduce the pressure in the fracture, increase the effective pressure gradient, and enhance the potential utilization of adsorbed gas as soon as possible to increase the ultimate recovery. The findings of this study can help for a better understanding of the shale reservoir utilization law so as to provide a reference for production optimization and development plan formulation of the shale gas reservoirs.

1. Introduction

Shale is a potentially unconventional gas reservoir, both the source rock and the storage space for shale gas. Different from the gas occurrence of conventional gas reservoirs, shale gas is mainly composed of free gas and adsorbed gas. Specifically, free gas mainly occurs in the fractures, matrix pores, or organic nanopores of shale reservoirs, and adsorbed gas mainly exists in kerogen, clay particles, and pore surfaces [1, 2]. The adsorbed gas proportion in different shale gas fields universally lies between 20% and 80% [3]; thus, studying the production performance of shale gas in different occurrence states is of great significance for enhancing shale gas development efficiency [4, 5]. Due to the extremely low porosity and low permeability of shale reservoirs and the complex gas occurrence-transport conditions, the shale gas flow mechanism is very complicated, dominated by coupled effects of viscous flow, slip, diffusion, and desorption resulting in the fact that the conventional gas flow equation cannot be applicable to shale gas reservoirs. The shale gas

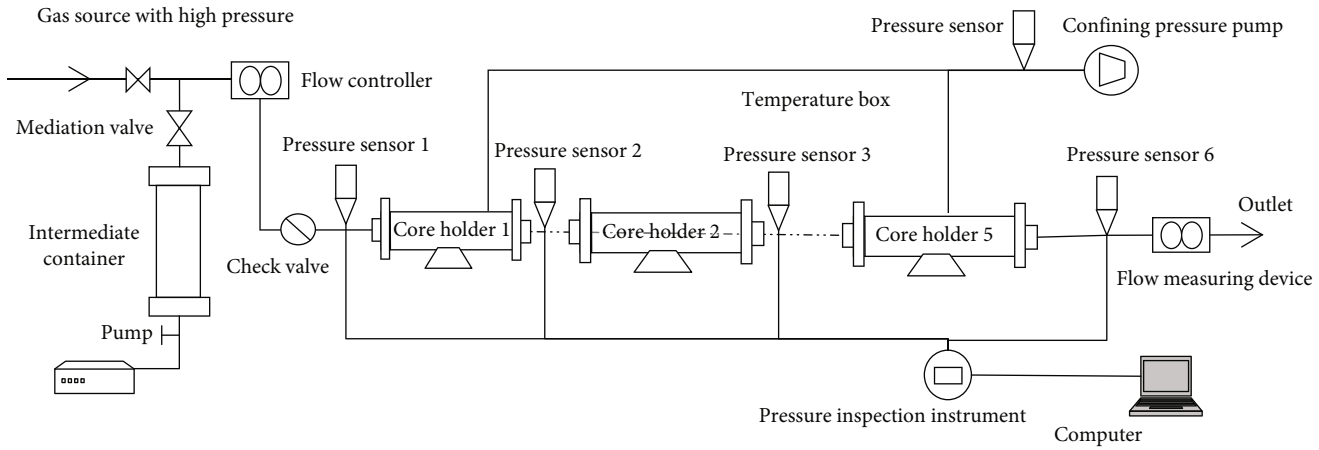

Figure 1: Flow chart of coupled flow experiment device.

production curve has unique L-shaped production characteristics, with high initial production, rapid decline rate, and long stable production period in the later period [6, 7]. The pressure and production data are only adopted to predict production using experience or semiexperience, which cannot reasonably explain the large difference in single well production of shale gas and illustrate the unclear decline rate performance, restricting the efficient development of shale gas to a certain extent [8].

The current research on shale gas development is mostly based on the production data analysis and prediction of shale gas wells [9–11], restricted by the discontinuous production data, short single well production time, and inaccurate production forecasts. Thus, the physical simulation experiment on the shale gas utilization mechanism and development rules is conducted in the paper. The indoor shale gas research mainly focuses on the static evaluation of reservoir physical properties, such as shale gas porosity, permeability test and pore connectivity characterization [12–14], and adsorption isotherm curve test for adsorbed gas volume [15, 16]. It can be seen from the previous studies that there are relatively few studies on the shale gas dynamic production performance, mostly focusing on theoretical models and numerical simulations [17–20]. The physical simulation experiments for shale gas development dynamics are rare in the literature.

Therefore, considering the unclear understanding of the gas generation mechanism and production law of shale gas reservoirs, the workflow is developed as follows: first, the self-developed high-precision, multipoint depletion development simulation experiment system was adopted to carry out the natural depletion simulation for shale sample, coal samples, and tight sandstone samples, respectively, to obtain a qualitative understanding of the gas output law of different occurrence states. Then, combined with isothermal adsorption experiments, material balance equations, and one-dimensional flow model, the utilization mechanism and development rules of free gas and adsorbed gas were analyzed, which can provide a reference for production optimization and development plan formulation of the shale gas reservoirs.

2. Experimental Design

Due to the limited gas supply range of the matrix, the shale gas reservoir is transformed into the "artificial gas reservoir" by hydraulic fracturing, where gas flow channels are established, and then, depletion depressurization is adopted [1]. Since artificial fracture conductivity is much greater than that of the matrix, the gas supply capacity in the matrix is very important to the stable production period of the gas well [17] after the fracturing fluid and gas are produced in the artificial fractures. The gas flow from the matrix to the complex fracture network plays a key role in the long-term stable production period of shale gas wells. A physical simulation of shale gas matrix supply is established by using multiple tandem cores (Figure 1) to simulate the gas one-dimensional flow from the matrix to the fracture near the fracture surface. The pressure propagation distance in the matrix can be directly obtained by setting pressure measurement points along the flow path. According to the gas production behavior and pressure profile, the gas utilization rate of the matrix blocks at different depths from the fracture surface can be calculated.

2.1. Experimental Samples. The shale samples were selected from the Long-1 submember of the Longmaxi Formation in the Sichuan Basin. In order to compare the difference of adsorption capacities on pressure propagation and gas production, coal samples with large adsorption capacity and tight sandstone with minimal adsorption capacity were chosen for comparison experiments. Specifically, the coal samples were taken from coal seams in the Qinshui Basin, and the tight sandstones were artificially compressed quartz sand samples. The detailed parameters of the experimental rock samples are shown in Table 1. The GAI-100 high-pressure isotherm gas adsorption of the American CORELAB company [21] is adopted to obtain the adsorption isotherm curves. Methane with a purity of 99.99% is used as the test gas in the experiment to truly reflect the flow state of shale gas.

2.2. Developed Simulation Experiment Methods. The self-developed multipoint depletion development simulation experiment system mainly includes ISCO pumps, high-

Table 1: Basic physical parameters of experimental samples.

	Core number	Length (cm)	Diameter (cm)	Porosity (%)	Permeability (mD)
Shale	1	3.81	2.54	2.01	0.00032
	2	3.73	2.54	2.3	0.0011
	3-1	3.17	2.50	1.86	0.00016
	3-2	4.36	2.54	2.40	0.0002
	3-3	4.12	2.53	1.77	0.00011
	3-4	3.10	2.50	2.08	0.00026
	3-5	4.43	2.51	1.70	0.00056
Coal sample	4-1	6.11	3.81	6.82	0.039
	4-2	6.13	3.82	7.51	0.015
	4-3	6.44	3.81	6.96	0.011
	4-4	4.35	3.82	9.82	0.15
	4-5	4.93	3.81	9. 01	0.19
Tight sandstone	5-1	4.21	3.81	9.83	0.0015
	5-2	4.47	3.84	11.21	0.0048
	5-3	4.27	3.84	12.88	0.0063
	5-4	4.28	3.80	13.55	0.011
	5-5	4.34	3.81	14.42	0.016

pressure volume flow meters, high-precision pressure sensors, core holders, intermediate vessels, ring pressure pumps, and methane explosion-proof detection devices.

The experimental process is as follows: (1) First, the airtightness of the system needs to be checked; then, the core can be dried at 105°C for 48 hours and cooled at room temperature in a dry environment, finally put into the holder, adding confining pressure to 35 MPa. (2) The reservoir has to be restored in the original pressure state; then, methane gas is injected into the core in constant pressure, and the pressure at each measurement point is recorded. When the pressure at each measuring point of the core is saturated to 30 MPa, the gas source needs to be closed, and then, the pressure at each measuring point is observed. If the pressure at each measuring point fluctuates less than 0.01% within 96 hours, the core is considered to be fully saturated. (3) The outlet is opened, the exhaustion development experiment is started, and the pressure of each measuring point and the gas production data at the outlet are recorded in real time.

The following designs were made to improve the accuracy of the experiment: (1) The free volume of the system is reduced. Due to the small porosity of shale, the free volume in the experimental system, including the free volume in the pipelines, valves, and holder channels, cannot be ignored in the experimental gas content and gas production. In particular, the core holders with small free customization are adopted in the experiment, and fillers are added in pipelines and valves to minimize the free volume. Furthermore, the gas expansion method is used to accurately measure the free volume of the system and deduct it from the calculation of the gas volume. (2) For the stage-measured pressure and flow rate method, since the pressure in the depletion development experiment covers a large span of the original formation pressure to the wasted formation pressure, pressure sensors with different ranges are selected to ensure the accuracy of the measurement. The imported gas mass flow meters are employed in the fast initial flow rate, while the bubble method or micropipe drainage method for multiple measurements is adopted in the low-yield period. (3) The experiments with different gases and different scales of cores can be conducted by the experimental system. Six pressure measuring points are set between the inlet, outlet, and the holder totally in the depletion development experiment of multiple tandem cores, which can measure the pressure of the core production process to obtain the pressure profile.

3. Results and Analysis of Development Simulation Experiment

3.1. Analysis of Pressure Spreading and Gas Production Performance. The multipoint depletion development simulation experiment can directly measure the pressure at different distances from the fracture surface and obtain the pressure propagation profile of the matrix and the gas production rate and cumulative gas production data. The pressure profile and gas production of shale samples measured at different production times are shown in Figures 2 and 3.

It can be seen from Figure 2 that the average matrix permeability of this group of cores is 0.00025 mD, the total length of cores is about 20 cm, and the experimental gas production time lasts for 315 days. The gas production is still ongoing. The pressure at the inlet drops from the initial pressure of 30 MPa to 9.7 MPa. At the initial development stage, the pressure profile detected at each measurement point is the same as that of conventional gas reservoirs such as sandstone, and the dynamic boundary presents an "upward convex" pressure drop funnel. The closer

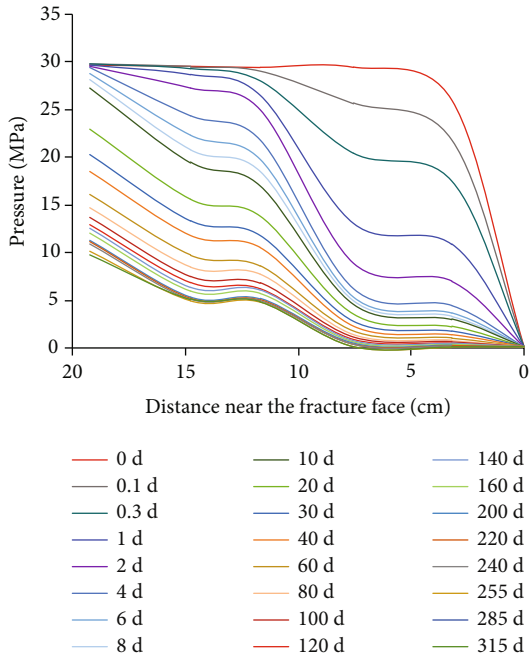

Figure 2: Pressure profile curve with production time.

production outlet can lead to the greater pressure drop, and the time that the pressure spreads to the boundary (No. 1 pressure measuring point) is about 6 days. As the production time progresses, the pressure at each measuring point gradually decreases. When the pressure drops to about 15 MPa, the pressure profile gradually changes from "upward convex" to "downward concave," due to the fact that the large supply of adsorbed gas has slowed down the pressure drop in the low-pressure area near the outlet, while the adsorbed gas at the remote pressure measuring point has not yet been utilized, and thus, the free gas is mainly produced. The pressure drop is slower during the later stage of production. Therefore, the low-stable production period can last for several years or even more than ten years in the shale gas reservoirs [22–24].

From the logarithmic coordinate of the gas production rate curve (Figure 3), it can be seen that the gas production rate dropped rapidly from 3.4 L/d to below 0.1 L/d within 10 days of the initial production period, and the gas production rate can be stable from 0.001 L/d to 0.01 L/d for more than 300 days, entering a long period of low-stable production. The current cumulative gas production is 1.39 L; the high initial gas production rate and the rising cumulative gas production curve can be illustrated by the free gas produced mainly under high pressure .

The same experimental procedure was adopted to analyze the influence of adsorbed gas on pressure propagation and gas production. A comparison experiment was carried out on tight sandstone without adsorbed gas and coal samples with an adsorbed gas ratio of more than 50%. The pressure profile of tight sandstone tandem cores and coal tandem core depletion development is shown in Figure 4.

As is shown in Figure 4(a), the pressure propagation of tight sandstone to the boundary (31 cm) lasts for less than 0.2 h, and the experimental pressure has dropped below 7 MPa within 4.8 h. The average permeability of tight sandstone is about 0.008 mD, which is about 30 times larger than that of shale, leading to a relatively fast gas production rate. There only exists free gas in tight sandstone samples, and the adsorbed gas is basically negligible. Thus, the produced gas is mainly free gas from tight sandstone. The pressure profile is a conventional pressure drop funnel. The gas closer to the fracture surface is extracted more easily.

Relatively speaking, the gas in coal samples mainly exists as adsorbed gas, accounting for about 70%. The tested permeability of coal samples is relatively higher than that of tight sandstone and shale samples, with an average value of 0.08 mD. Due to the high complexity, heterogeneity of the coal structure, and the large range of the pore size distribution, large pores and many cracks become the main flow channel. Therefore, the initial pressure drops below 12 MPa relatively quickly within 1.4 days. A large amount of adsorbed gas in the coal sample matrix can obviously slow the pressure drop when desorption occurs. The supply of adsorbed gas guarantees the coal gas a long-term stable production period. Specifically, the pressure change becomes smaller in the later production period, except for the relatively large pressure drop near the outlet. Then, the trend from "upward convex" to "downward concave" is very obvious, and the supply of adsorbed gas makes the pressure profile smoother in the later stage.

The cumulative gas production and cumulative gas recovery curves of the three samples are compared, and the results are shown in Figure 5.

It can be seen from Figure 5 that the initial gas rates of the three samples are relatively high. The gas recovery rate of tight sandstones has risen rapidly to over 90% in a short period of time, indicating that the free gas in sandstones can easily be destroyed as the pressure decreases. Compared with tight sandstone, the recovery rate of shale gas and coal are, respectively, 70% and 90%. The recovery of shale and coal has a slower rise. The main reason is that after the initial free gas is extracted, it needs to rely on the supply of adsorbed gas desorption, the desorption of adsorbed gas is a slow process, so the degree of recovery slowly increases.

The relationship curve between the cumulative gas production and the apparent pressure of the three samples can be seen that when the pressure is relatively high, the cumulative gas production increases linearly with the decrease in the apparent pressure during the initial development period, which is consistent in the relationship between the free gas and the apparent pressure, indicating that the free gas is mainly produced in the early stage of development, the adsorbed gas in the later stage of production makes the gas production curve of shale and coal deviate from the linear relationship, and the amount of adsorbed gas is largest in the coal [25]. The deviation from the linear relationship of cumulative gas production can be indicated by the adsorbed gas. Even though there is a difference in the physical properties of the three different rock samples, the permeability of the coal sample is the largest, followed by tight sandstone

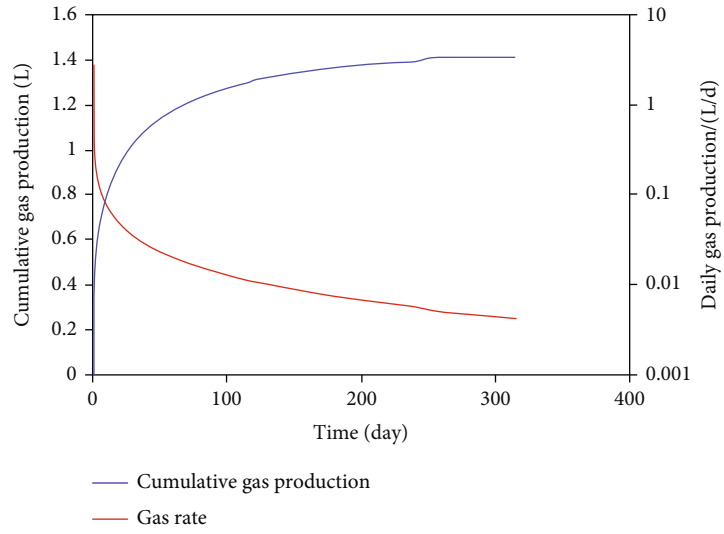

Figure 3: Gas production and gas production rate versus production time.

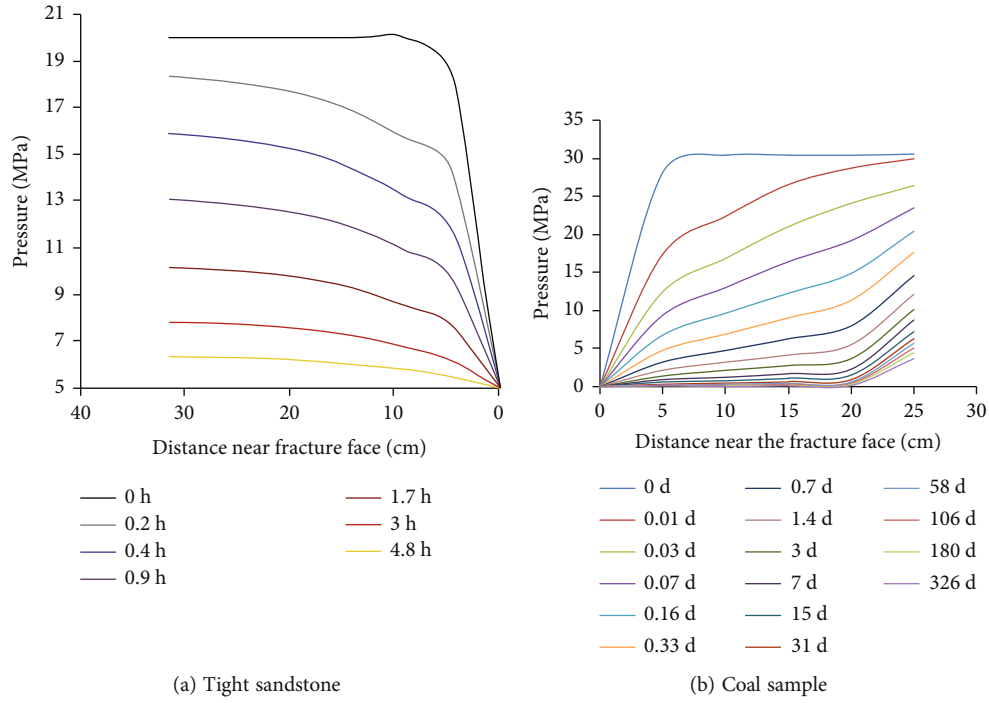

(a) Tight sandstone (b) Coal sample

Figure 4: Pressure profile curve of tight sandstone and coal.

and shale. The difference in the gas occurrence state leads to different gas production performances, in which the pressure drop rate is ranked as tight sandstone > shale > coal sample for the difference in the adsorbed gas ratio for each sample. The gas production curve per unit pressure drop under different pressure conditions is summarized as shown in Figure 6.

The gas production per unit pressure drop represents the gas production for each average pressure drop pressure in the core system. Figure 6 shows that the gas production rates of three samples maintained stable in the initial production stage. When the pressure drops to a certain level, the gas production per unit pressure drop of tight sandstones without adsorbed gas basically does not change, while the gas production per unit pressure drop of shale and coal seams with adsorbed gas rises significantly, indicating that the adsorbed gas begins to desorb and becomes produced free gas. The greater amount of adsorbed gas can lead to a more obvious increase.

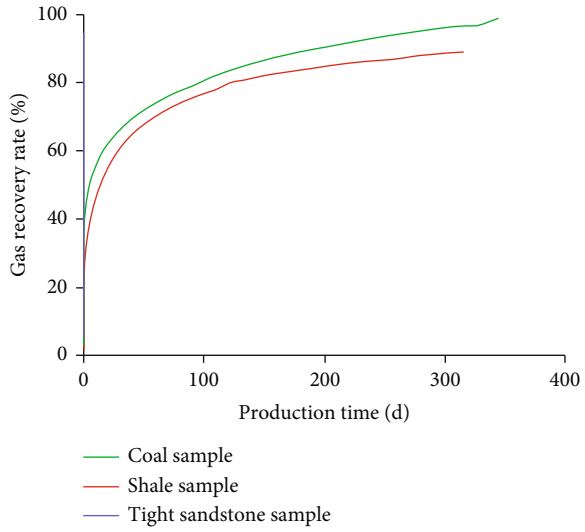

Figure 5: Gas recovery rate versus production time.

3.2. Adsorption and Free Pneumatics Characteristics

3.2.1. Shale Gas Material Balance Theoretical Model. According to the relationship curve of formation pressure, cumulative gas production, and daily gas production with the decrease of formation pressure, combined with the relevant theory of gas reservoir engineering, the amount of free gas and adsorbed gas production can be estimated to further analyze the production law of free gas and adsorbed gas [26, 27]. The shale sample contains free gas and adsorbed gas, of which the free gas volume is calculated by pore volume and volume coefficient, and the adsorbed gas volume is calculated using the corrected Langmuir adsorption formula [16]. The reserve calculation formulas are as follows.

The original free gas volume G_{f0} of the matrix:

$$G_{f0} = \frac{V\phi_M}{B_{g0}}. \tag{1}$$

The original adsorption gas G_{ad0}:

$$G_{ad0} = V_M * V_L \frac{p}{p_L + p}\left(1 - \beta\rho_g\right). \tag{2}$$

Reduction in the free gas and adsorbed gas amount at time t:

$$G_{free} = V\phi_M \frac{T_{sc}P_i}{TZ_iP_{SC}} - V\phi_M \frac{T_{sc}P}{TZP_{SC}},$$
$$G_{ab} = M_0 * V_L \frac{p_i}{p_L + p_i}\left(1 - \beta\rho_{gi}\right) - M_0 * V_L \frac{p}{p_L + p}\left(1 - \beta\rho_g\right). \tag{3}$$

The cumulative gas production is

$$G_t = G_{free} + G_{ab}. \tag{4}$$

Based on the material balance equation for closed gas reservoirs, without considering the adsorbed gas, the apparent formation pressure decreases linearly with the increase of free gas production, which can be expressed as equation (5) [28]:

$$G_{free} = G_0\left(1 - \frac{Z_iP}{ZP_i}\right). \tag{5}$$

The above expression shows that the slope of the early shale gas cumulative gas production and apparent pressure curve is G_0Z_i/P_i, and the intercept is the total free gas content G_0. Therefore, the total free gas volume G_0 can be determined by the slope of the early shale gas cumulative gas production and the apparent pressure curve. The relationship between adsorbed gas volume, free gas volume, and total gas volume in shale is shown in Figure 7.

Figure 7 shows that the cumulative gas production curve calculated by the model has a good fitting result with the measured results, and the calculated adsorbed gas and free gas volume are testified to be reliable. It can be seen from Figure 8 that the cumulative gas production curve is consistent with the free gas content in the high pressure and has a good linear relationship with the apparent average pressure. The free gas content estimated by the linear section of the cumulative gas production is about 1.4 L, slightly larger than that calculated by the core porosity, that is, 1.36, due to a small amount of desorbed gas near the outlet end. The lower pressure leads to higher adsorbed gas production and the increased contribution to the cumulative gas production. Thus, the cumulative gas production curve deviates from the straight line, and the free gas volume and the apparent pressure show a good linear relationship.

It can be seen from Figure 7 that during the production time of more than 300 days, the total recovery rate is about 70%. It is mainly contributed by free gas, which currently accounts for more than 90% of the total gas production. Especially during the initial 30 days of development, the average pressure of the core is higher than 10 MPa, when free gas is mainly produced, accounting for more than 90% of the total gas production. During the production process, the pressure decreases, and the adsorbed gas recovery rate gradually rises. The absorbed gas and free gas recovery rates of 5 cores with different distances from the fracture surface are, respectively, calculated, as shown in Figure 9. No. 5 is the core closest to the fracture surface, the other numbers are sequentially away from the fracture surface, and No. 1 is the most remote end.

It can be seen from Figure 9 that the free gas and adsorbed gas of core No. 5 near the outlet end have the highest recovery rate. The aerodynamics law of free gas is relatively clear: a large amount of free gas begins to be produced as the pressure decreases, and the distance closer to the fracture surface in the core can result in a higher recovery rate, while the amount of adsorbed gas

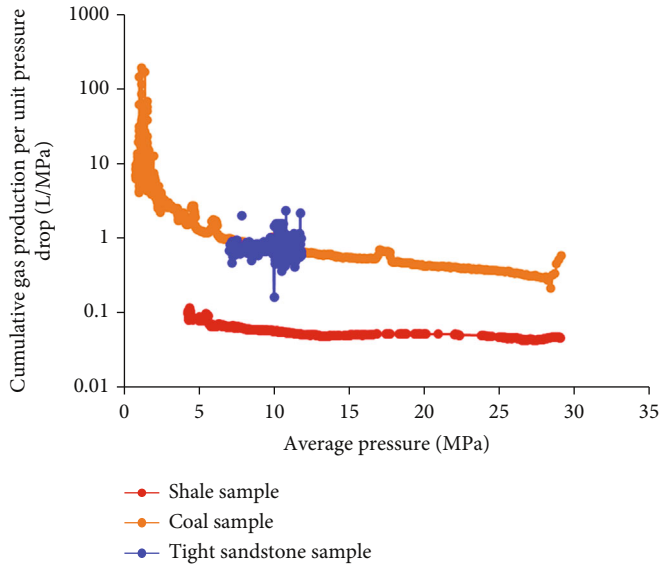

Figure 6: Comparison of gas production per unit pressure drop of three samples.

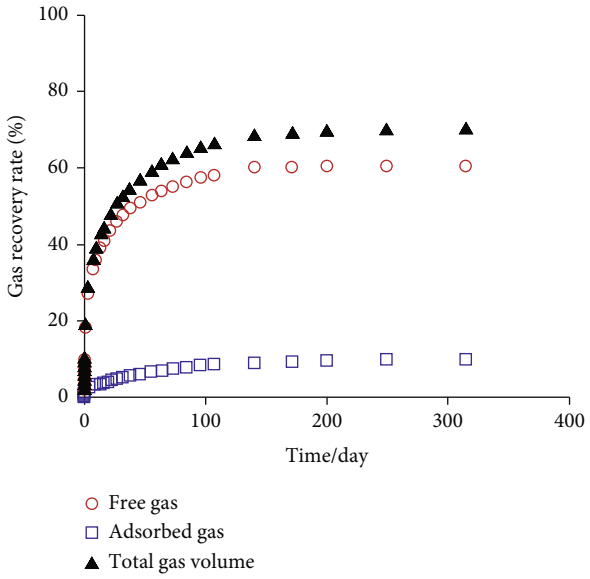

Figure 7: Gas recovery rate versus production time.

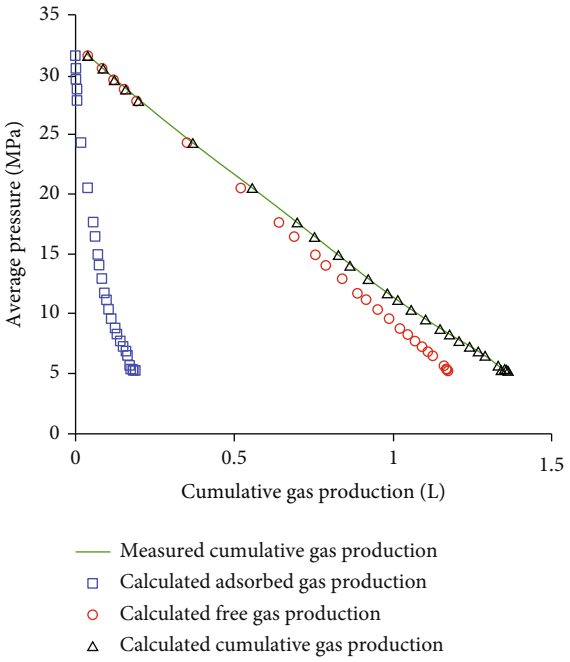

Figure 8: The relationship between the calculated gas production and apparent pressure.

production is very small, mainly in the low-pressure area near the outlet. Core No. 5 has the highest proportion of adsorbed gas utilization, accounting for about 70%, while the pressure of core No. 1 at the far end still stays above 10 MPa, and the proportion of adsorbed gas utilization is small, which is less than 5%. In actual production, free gas is mainly produced in the matrix far from the fracture surface with less absorbed gas, while the production of adsorbed gas mainly occurs in the later stage of production. The lower pressure can promote the production of more adsorbed gas in the later stage.

The high-pressure isothermal adsorption curves of two shale samples in Changning and Weiyuan are shown in Figure 10 The static high-pressure isothermal adsorption experiment also confirmed that the adsorbed gas has a critical desorption pressure [16]. When the adsorption becomes saturated during the pressurized process, there is a maximum of the excess adsorption, indicating the maximum adsorption capacity of the adsorbed layer and the corresponding pressure is the critical desorption pressure. When the formation pressure is higher than the critical desorption pressure, the adsorption layer is saturated, the adsorption phase density tends to be stable, and the adsorbed gas volume maintains stable. Since the adsorption layer is saturated

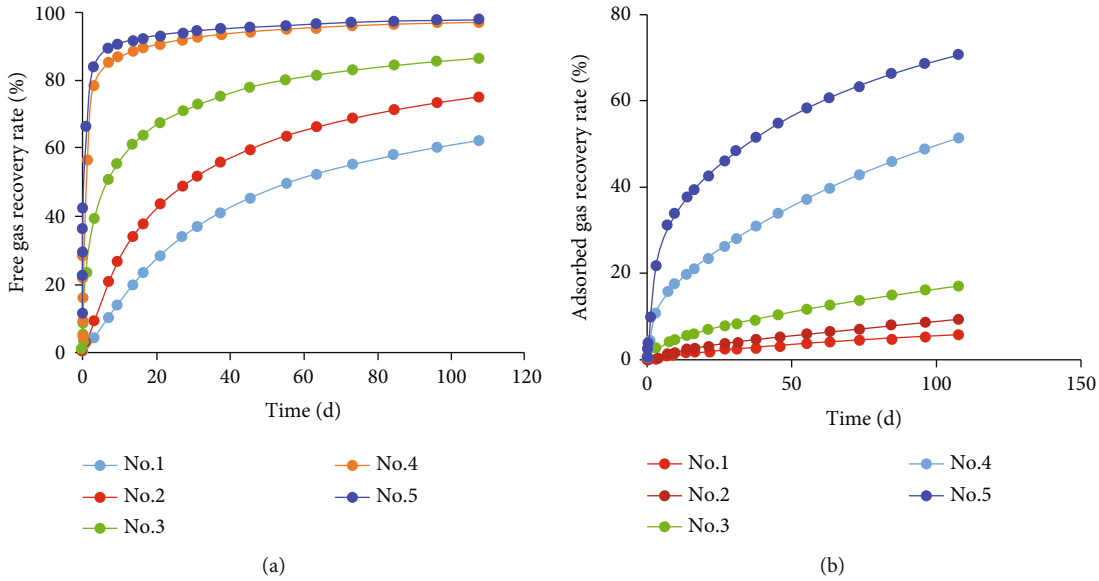

Figure 9: The free gas and adsorbed gas recovery rate from matrix blocks at different distances from the fracture surface.

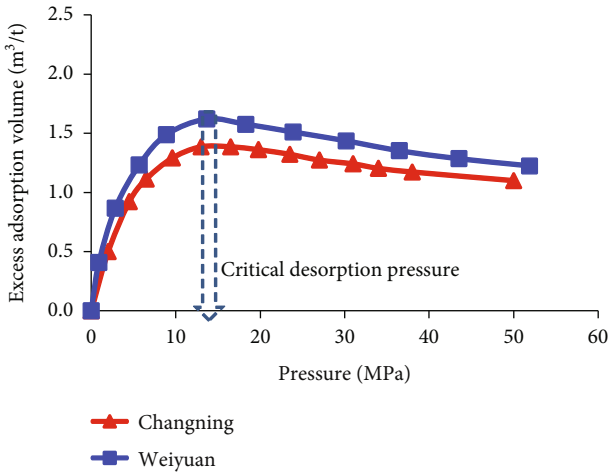

Figure 10: Critical desorption pressure in adsorption isotherm curve.

at about 12-15 MPa, the critical desorption pressure of shale samples can be accurately determined through high-pressure isothermal adsorption experiments. Only in the dynamic production simulation experiment can the adsorbed gas production law be described more accurately.

3.2.2. Shale Gas One-Dimensional Flow Model Research

(1) Model Building. Combining the mass conservation equation and the equation of motion, a one-dimensional flow productivity model of shale gas is established to simulate the real reservoir gas production characteristics and to study the contribution of adsorbed gas to gas production. On the basis of the conventional three-zone seepage model, the high-pressure gas physical property nonlinearity, high-pressure isothermal adsorption model, the apparent permeability model of gas diffusion and slippage under low pressure, and the exponential stress sensitivity in the secondary fracture network are comprehensively considered in the improved one-dimensional seepage model in the paper as shown in Figure 11.

The specific assumptions are as follows:

(a) A quarter of a single fracture in the SRV area is selected as shown in Figure 11. The convergence of shale gas from the reservoir to the wellbore is a one-dimensional seepage process of single-phase methane gas in the three seepage fields, and the outer boundary of the shale reservoir is homogeneous and equally thick

(b) The occurrence state of the gas in the matrix includes free phase and adsorbed gas. The adsorbed gas on the pore wall of the matrix satisfies the supercritical Langmuir adsorption equation, and the diffusion and slippage of free gas in the micro-nanopores of the matrix are considered

(c) The gas in the fracture network area only exists in a free gas state. Considering the stress sensitivity of the fracture network, the gas is supplied to the main fracture direction in the fracture network

(d) The main fractures in the inner zone are uniformly distributed, have equal length, are symmetrical up and down, and fully compress the reservoir vertically. The half-length of the main fracture is y_F, the fracture width is w, the main fracture cluster spacing is L_F, the width of the main fracture is d, and the gas flow behavior follows Darcy's law

(e) The channeling of gas between different seepage areas is an unsteady and isothermal flow, ignoring

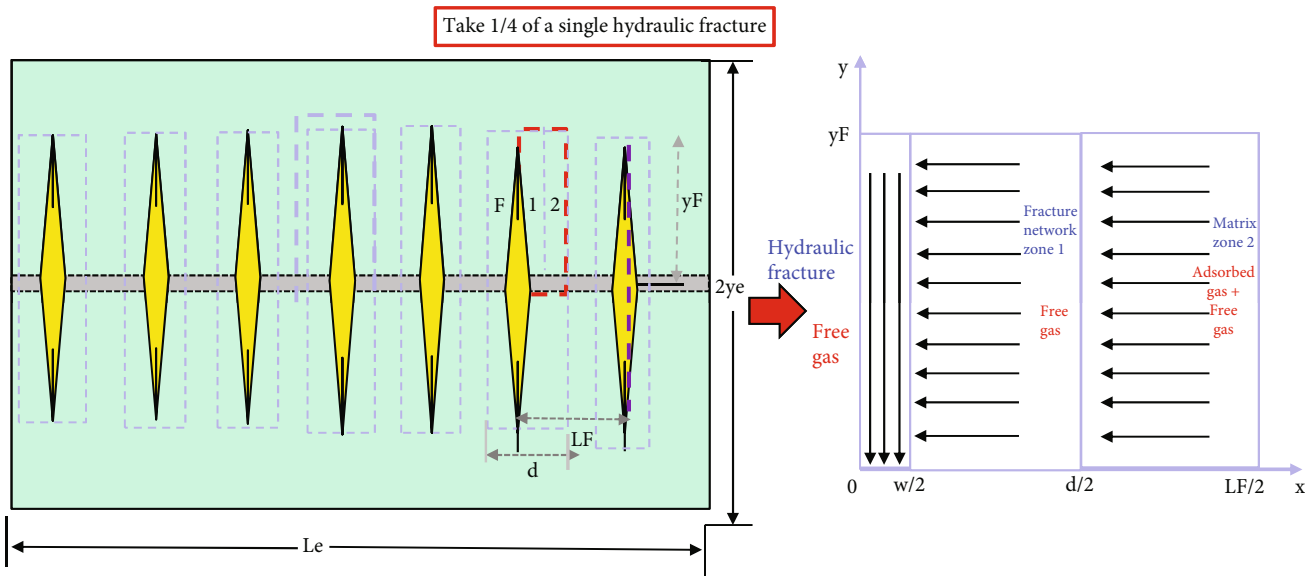

Figure 11: One-dimensional seepage physical model of shale gas fractured horizontal well.

Table 2: Dimensionless parameter definition.

Dimensionless parameter	Definition	Dimensionless parameter	Definition
Dimensionless pseudopressure	$\psi_D = \psi_i - \psi/\psi_i - \psi_{wf}$	Dimensionless production	$\frac{1}{q_D} = \frac{T_{sc}K_F\sqrt{A_{cw}}\left(\psi_i - \psi_{wf}\right)}{P_{sc}q_{sc}T}$
Dimensionless pseudotime	$t_{aD} = \frac{K_F t_a}{\mu\left(\varphi_m C_{tm} + \varphi_f C_{tf} + \varphi_F C_{tF}\right)A_{cw}}$	Storage capacity ratio in the matrix	$w_m = \frac{\psi_m C_{tm}}{\varphi_m C_{tm} + \varphi_F C_{tF} + \varphi_f C_{tf}}$
Dimensionless length	$x_D = \frac{2x}{L_f}, y_D = \frac{y}{\sqrt{A_{cw}}}$	Storage capacity ratio in the fracture network	$w_f = \frac{\psi_f C_{tf}}{\varphi_m C_{tm} + \varphi_F C_{tF} + \varphi_f C_{tf}}$
Zone f-F mass transfer coefficient	$\lambda_{fF} = \frac{12K_f}{L_F^2 K_F}A_{cw}$	Storage capacity ratio in the hydraulic fracture	$w_F = \frac{\psi_F C_{tF}}{\varphi_m C_{tm} + \varphi_F C_{tF} + \varphi_f C_{tf}}$
Dimensionless conductivity in the matrix	$\eta_{mD} = \frac{K_F}{\varphi_m C_{mt} + \varphi_f C_{tf} + \varphi_F C_{tF}}\frac{\varphi_m C_{tm}}{K_{ma}}$	Dimensionless formation conductivity	$R_{CD} = \frac{K_f d}{K_m L_F}$
Dimensionless pressure	$\gamma_{fD} = \gamma_f\left(\psi_i - \psi_{wf}\right)$		

gravity and capillary force. The shale gas well is working at constant pressure

Based on the dimensionless parameter definitions in Table 2, the simplified dimensionless flow equation in the matrix is depicted in

$$\begin{cases} \dfrac{\partial \psi_{mD}}{\partial t_{aD}} = \dfrac{1}{\eta_{mD}}\dfrac{\partial^2 \psi_{mD}}{\partial {x_D}^2}, \\ \psi_{mD}(x_D, 0) = 0, \\ \psi_{mD}\left(\dfrac{d_D}{2}, t_{aD}\right) = \psi_{fD}\left(\dfrac{d_D}{2}, t_{aD}\right), \\ \dfrac{\partial \psi_{mD}(d_D/2, t_{aD})}{\partial x_D}\Big|_{x_D=1} = 0. \end{cases} \tag{6}$$

Likewise, the dimensionless flow equation in the fracture network is depicted in

$$\begin{cases} \dfrac{\partial^2 \psi_{fD}}{\partial {x_D}^2} - \gamma_{fD}\left(\dfrac{\partial \psi_{fD}}{\partial x_D}\right) = \dfrac{3w_f}{\lambda_{fF}e^{\gamma_{fD}\cdot\psi_{fD}}}\dfrac{\partial \psi_{fD}}{\partial t_{aD}}, \\ \psi_{fD}(x_D, 0) = 0, \\ \psi_{fD}(0, t_{aD}) = \psi_{FD}, \\ \dfrac{\partial \psi_{fD}(x_D, t_{aD})}{\partial x_D}\Big|_{x_D=d_D/2} = \dfrac{e^{\gamma_{fD}\cdot\psi_{fD}}d_D}{2R_{CD}}\dfrac{\partial \psi_{mD}(x_D, t_{aD})}{\partial x_D}\Big|_{x_D=d_D/2}. \end{cases} \tag{7}$$

Similarly, the dimensionless flow equation in the hydraulic fracture is depicted in

Table 3: Model fitting parameters.

Parameter name	Value	Parameter name	Value
Initial pressure (MPa)	30	Matrix average porosity	0.056
Experimental temperature (K)	300	Matrix average permeability (mD)	0.000647
Core length (cm)	50	Langmuir volume (m^3/t)	4.7
Core diameter (cm)	2.5	Langmuir pressure (MPa)	8.5
Rock density (kg/m^3)	2600	Constant pressure in the outlet (MPa)	3
Stress sensitivity coefficient (MPa^{-1})	0.13		

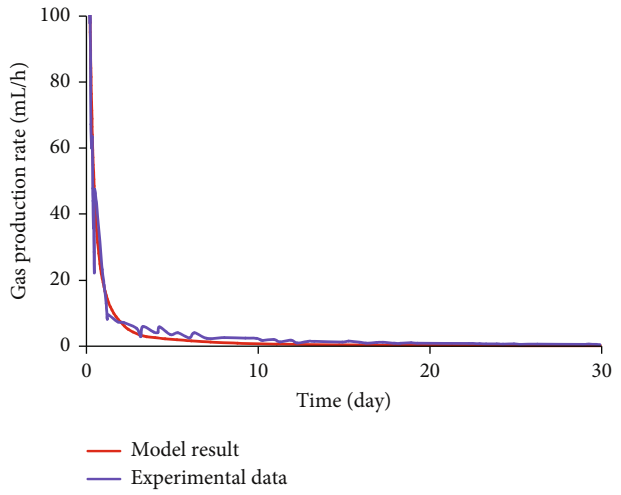

Figure 12: Fitting results of gas production rate of tandem cores.

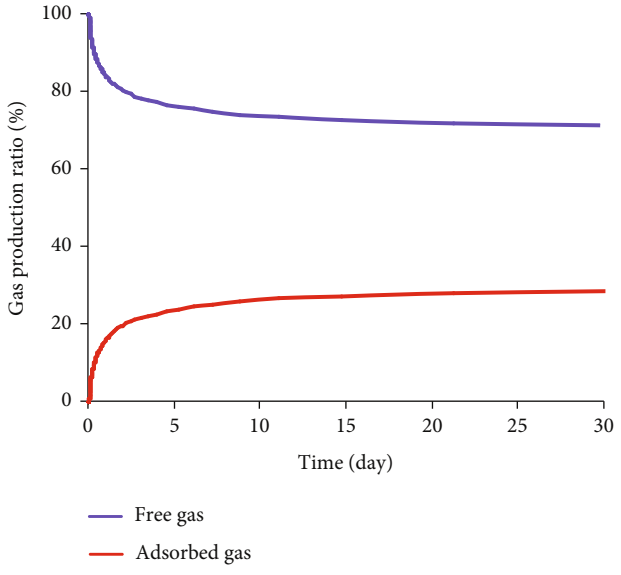

Figure 13: The gas production proportion of tandem cores versus time.

$$\begin{cases} \dfrac{\partial^2 \psi_{FD}}{\partial {y_D}^2} = w_F \dfrac{\partial \psi_{FD}}{\partial t_{aD}} - \dfrac{\lambda_{fF} e^{\gamma_{fD} \cdot \psi_{fD}}}{3} \dfrac{\partial \psi_{fD}}{\partial x_D} \Big|_{x_D = d_D/2}, \\ \psi_{FD}(y_D, 0) = 0, \\ \psi_{FD}(0, t_{aD}) = 1, \\ \dfrac{\partial \psi_{FD}(y_D, t_{aD})}{\partial t_{aD}} \Big|_{y_D = y_{FD}}. \end{cases} \tag{8}$$

The dimensionless seepage mathematical equations can be solved by Laplace transformation in Laplace space; then combined with the Stehfest numerical inversion and Newton iteration method, the production solution in real space is obtained during constant pressure production.

(2) Case Study. Considering that the pressure distribution data at different venting radii in the production process by a single core cannot be obtained, five cores connected in series were designed for depletion development simulation to validate the proposed production prediction model and basic model fitting parameters which are shown in Table 3. Figure 12 shows that the experimental data and model results fit well, and the experimental results show that the 30-day total gas production volume is 3.39 L, compared to the model calculation results of the gas production volume 3.423 L, with the relative error of less than 5%, which can prove the reliability of the model.

As is shown in Figure 13, the desorption effect becomes more significant with the increase of the experiment time, and the proportion of desorption gas can ultimately reach 28.63%. The apparent formation pressure decreases with the increasing time promoting the occurrence of gas desorption, and the proportion of desorbed gas increases in gas production composition.

It can be seen that the gas production is dominated by free gas in the shale gas reservoirs of high reservoir pressure coefficient and high proportion of free gas while adsorbed gas becomes important only when the reservoir drops below the critical pressure. As for gas reservoirs dominated by adsorbed gas, depressurization development is the main method, characterized by the low gas production rate and the long stable production time; thus, adsorbed gas is the main source of long-term stable production in the later stage. Therefore, shale gas development is recommended to achieve "effective control and efficient production"; that is,

to maximize the volume of shale matrix that can be communicated by fractures, shorten the supply distance of the matrix, and ensure that the recoverable reserves in the SRV area are "effectively controlled" by the fractures to increase the utilization rate of reserves. Meanwhile, it is necessary to reduce the pressure as much as possible, increase the effective pressure gradient, and ensure the "efficient production" of free gas and adsorbed gas. When the gas reservoir pressure drops below the critical desorption pressure, the adsorbed gas starts to be supplied, the gas production per unit pressure drop rises rapidly, and the gas production increases rapidly. The pressure reduction increases the gas diffusion, and the gas flow capacity is relatively enhanced, thereby increasing the single well production and final recovery rate.

4. Summary and Conclusions

(1) The difference in gas occurrence state is the main factor of the different gas production laws of the shale, coal seams, and tight sandstone. In the permeability experiment, the coal sample > tight sandstone > shale, while the pressure drop rate of tight sandstone is the largest, followed by shale and coal sample. The large amount of adsorbed gas delays the pressure drop rate of coal and shale and greatly prolongs the low-stable production period

(2) Unlike free gas, there is a critical desorption pressure for adsorption pneumatics. Both static and dynamic experiments have confirmed that the critical desorption pressure for adsorption pneumatics is generally 12-15 MPa. Due to the slow propagation of shale matrix flow pressure, when the reservoir pressure is higher than the critical desorption pressure in the initial high production stage, free gas is mainly produced, and there exists a linear relationship between gas production and the apparent pressure, which can contribute more than 90% to the initial production

(3) It can be seen from the pressure profile that adsorption pneumatics mainly occur in the low-pressure area near the fracture surface. The material balance theory of closed gas reservoirs and the one-dimensional flow model of shale gas are used to study the production performance of adsorbed gas and free gas: when the formation pressure is below the critical desorption pressure, the adsorbed gas starts to be produced in large quantities, and the gas production per unit pressure drop rises rapidly, resulting in stable production in the late development stage. Therefore, in practical development of shale gas reservoir, it is recommended to shorten the matrix supply distance, reduce the pressure in the fracture, increase the effective pressure gradient, and enhance the potential utilization of adsorbed gas as soon as possible to increase the ultimate recovery

Nomenclature

G_{f0}: Free gas reserves in the matrix (m^3)
G_{ad0}: Adsorbed gas reserves in the matrix (m^3)
P_i: Initial gas reservoir pressure (MPa)
V_L: Langmuir volume (m^3/t)
P_L: Langmuir pressure (MPa)
B_g: Volume factor, decimal
G_{free}: Free gas production at the time of t (m^3)
G_{ab}: Adsorbed gas production at the time of t (m^3)
P: Gas reservoir pressure at the time of t (MPa)
Z: The gas compression factor, dimensionless
Z_i: Initial gas compression factor, dimensionless
L_e: Effective horizontal length (m)
y_e: Reservoir width (m)
d: Fractured zone length (m)
y_F: Hydraulic fracture half-length (m)
L_F: Hydraulic fracture cluster spacing (m)
w: Hydraulic fracture width (m)
C_{tm}: The matrix comprehensive compressibility coefficient (Pa^{-1})
C_{tf}: The fracture network comprehensive compressibility coefficient (Pa^{-1})
C_{tF}: The fracture network comprehensive compressibility coefficient (Pa^{-1})
A_{cw}: Wellbore crossflow area (m^2)
K_m: The matrix permeability (mD)
K_f: The fracture network permeability (mD)
K_F: The hydraulic fracture permeability (mD)
P_{sc}: The standard atmospheric pressure, 0.101 (MPa)
T_{sc}: The standard temperature, 273.15 (K)
Z_{sc}: The ideal gas compressible factor, 1, dimensionless
γ_f: The pseudopermeability modulus ($Pa{\cdot}s/Pa^2$)
t_a: The pseudotime (s).

Greeks

φ_m: The matrix porosity, dimensionless
φ_f: The fracture network porosity, dimensionless
φ_F: The hydraulic fracture porosity, dimensionless
ψ_i: The initial formation pseudopressure ($Pa^2/(Pa{\cdot}s)$)
ψ_m: The matrix pseudopressure ($Pa^2/(Pa{\cdot}s)$)
ψ_f: The fracture network pseudopressure ($Pa^2/(Pa{\cdot}s)$)
ψ_F: The hydraulic fracture pseudopressure ($Pa^2/(Pa{\cdot}s)$)
ψ_{wf}: Bottom hole flowing pseudopressure ($Pa^2/(Pa{\cdot}s)$).

Data Availability

The data used to support the findings of this study are available from the corresponding authors upon request.

Conflicts of Interest

The authors declare that they have no conflicts of interest.

Acknowledgments

This research was funded by the China National Science and Technology Major Project Shale Gas Seepage Law and Gas Reservoir Engineering Method (Grant No. 2017ZX05037-001).

References

[1] C. Zou, Z. Yang, D. He et al., "Theory, technology and prospects of conventional and unconventional natural gas," *Petroleum Exploration and Development*, vol. 45, no. 4, pp. 604–618, 2018.

[2] X. Ma and J. Xie, "The progress and prospects of shale gas exploration and development in southern Sichuan Basin, SW China," *Petroleum Exploration and Development*, vol. 45, no. 1, pp. 172–182, 2018.

[3] J. B. Curtis, "Fractured shale-gas systems," *AAPG Bulletin*, vol. 86, no. 11, pp. 1921–1938, 2002.

[4] Z. Xuefen, X. Lu, Z. Linye, and L. Qin, "Research on the shale gas occurrence form and its petroleum geological significance," *Advances in Earth Science*, vol. 25, no. 6, pp. 597–604, 2010.

[5] S. L. Montgomery, D. M. Jarvie, K. A. Bowker, and R. M. Pollastro, "Mississippian Barnett Shale, Fort Worth basin, north-central Texas: gas-shale play with multi–trillion cubic foot potential," *AAPG Bulletin*, vol. 89, no. 2, pp. 155–175, 2005.

[6] B. Yuhu, C. Guihua, B. Xu, et al.F. Ruyong, and et al.C. Ling, "The typical curve model and comparative study of shale gas production decline," *China Petroleum Exploration*, vol. 21, no. 5, pp. 96–102, 2016.

[7] W. Zhu, D. Ma, Q. Qian, S. Zhiyong, and Y. Ming, "Multi-zone coupled productivity analysis of horizontal wells with complex fracture network," *Natural Gas Industry*, vol. 37, no. 7, pp. 60–68, 2017.

[8] Z. Xiaotao, C. Man, J. Xin, Y. Hongzhi, and Y. Xuefeng, "Research on productivity evaluation method of shale gas well," *Natural Gas Geoscience*, vol. 27, no. 3, pp. 549–553, 2016.

[9] R. G. Loucks and S. C. Ruppel, "Mississippian Barnett shale: lithofacies and depositional setting of a deep-water shale-gas succession in the Fort Worth Basin, Texas," *AAPG Bulletin*, vol. 91, no. 4, pp. 579–601, 2007.

[10] S. Yuliang, S. Guanglong, W. Wang, Y. Yi, and Z. Xuan, "A multi-media coupling flow model for shale gas reservoirs," *Natural Gas Industry*, vol. 36, no. 2, pp. 52–59, 2016.

[11] M. Lidong, J. Hanqiao, L. Junjian, and T. Ye, "Mathematical-characterization of permeability in shale reservoir," *Acta PetroleiSinica*, vol. 35, no. 5, pp. 928–934, 2014.

[12] P. H. Nelson, "Pore-throat sizes in sandstones, tight sandstones, and shales," *AAPG Bulletin*, vol. 93, no. 3, pp. 329–340, 2009.

[13] J. Zhijun, Z. Hu, B. Gao, and Z. Jianhua, "Shale gas enrichment and high production control factors of Wufeng-Longmaxi Formation in southeastern Sichuan," *Earth Science Frontiers*, vol. 23, no. 1, pp. 1–10, 2016.

[14] M. Gasparik, A. Ghanizadeh, P. Bertier, Y. Gensterblum, S. Bouw, and B. M. Krooss, "High-pressure methane sorption isotherms of black shales from the Netherlands," *Energy & Fuels*, vol. 26, no. 8, pp. 4995–5004, 2012.

[15] X. Duan, Z. Hu, S. Gao et al., "Shale high pressure isothermal adsorption curve and the production dynamic experiments of gas well," *Petroleum Exploration and Development*, vol. 45, no. 1, pp. 127–135, 2018.

[16] S. Gao, L. Huaxun, Y. Liyou, Z. Hu, and C. Jin, "A coupling model for gas diffusion and seepage in SRV section of shale gas reservoir," *Natural Gas Industry*, vol. 37, no. 1, pp. 97–104, 2017.

[17] F. Javadpour, "Nanopores and apparent permeability of gas flow in mudrocks (shales and siltstone)," *Journal of Canadian Petroleum Technology*, vol. 48, no. 8, pp. 16–21, 2009.

[18] Y. Wu, L. Cheng, H. Shijun, B. Yuhu, X. Bingxiang, and D. Guanyang, "Trilinear flow production prediction model of shale condensate gas wells," *Natural Gas Geoscience*, vol. 28, no. 11, pp. 1745–1754, 2017.

[19] T. Bolu, L. Cheng, H. Shijun, J. Zhen, and A. Shuang, "Shale gas reserve ultilization prediction based on wavefront rapid advancement method," *Journal of Southwest Petroleum University (Natural Science Edition)*, vol. 38, no. 2, pp. 122–128, 2016.

[20] C. Yaxing, X. Wei, Z. Hu, Z. Luo, and G. Shusheng, "Study on the apparent permeability of shale gas changing with pressure under isothermal conditions," *Natural Gas Geoscience*, vol. 28, no. 4, pp. 514–520, 2017.

[21] L. Taiwei, H. Guo, L. Haibo, L. Yan, and X. Xiaojia, "Study on movable fluids in shale gas reservoirs based on the nuclear magnetic resonance technology," *Special Oil and Gas Reservoirs*, vol. 19, no. 1, 2012.

[22] L. Biao, Y. Suping, W. Hu, C. Jian, and D. Delu, "Applicability of NMR freeze-thaw method to characterize pores in unconventional oil and gas reservoirs," *Acta Petrolei Sinica*, vol. 38, no. 12, pp. 1401–1410, 2017.

[23] R. J. Ambrose, R. C. Hartman, M. Diaz-Campos, I. Y. Akkutlu, and C. H. Sondergeld, "New pore-scale considerations for shale gas in place calculations," in *Proceedings of SPE Unconventional Gas Conference*, Allen, TX, USA, 2010.

[24] S. Gao, L. Huaxun, Y. Liyou, H. Zhiming, and A. Weiguo, "The physical simulation experiment and numerical inversion of entire life cycle for shale gas wells," *Acta Petrolei Sinica*, vol. 39, no. 4, pp. 435–444, 2018.

[25] W. Yunsheng, J. Ailin, H. Dongbo, W. Junlei, H. Pinlong, and J. Yiqiu, "Comparative analysis of development characteristics and technologies between shale gas and tight gas in China," *Natural Gas Industry*, vol. 37, no. 11, pp. 43–52, 2017.

[26] L. Zuo, Y. Wang, W. Xiong et al., "A new method to calculate the shale gas content," *Acta Petrolei Sinica*, vol. 36, no. 4, 2015.

[27] P. John, "Spivey," in *Gas Reservoir Engineering*, pp. 48–51, Petroleum Industry Press, 2011.

[28] X. F. Li, Y. C. Pu, C. Y. Sun et al., "Recognition of absorption/-desorption theory in coalbed methane reservoir and shale gas reservoir," *Acta Petrolei Sinica*, vol. 35, no. 6, pp. 1113–1129, 2014.